Available online at www.sciencedirect.com
ScienceDirect
Trans. Nonferrous Met. Soc. China 30(2020) 1429−1438
Transactions of Nonferrous Metals Society of China
www.tnmsc.cn

Effects of minor Sc and Zr additions on mechanical properties and microstructure evolution of Al−Zn−Mg−Cu alloys

Quan-feng XIAO[1], Ji-wu HUANG[1,2], Ying-ge JIANG[1], Fu-qin JIANG[1], Yun-feng WU[1], Guo-fu XU[1,2]

1. School of Materials Science and Engineering, Central South University, Changsha 410083, China;
2. Key Laboratory of Nonferrous Metallic Materials Science and Engineering, Ministry of Education, Central South University, Changsha 410083, China

Received 8 August 2019; accepted 30 April 2020

Abstract: The effects of minor Sc and Zr additions on the mechanical properties and microstructure evolution of Al−Zn−Mg−Cu alloys were studied using tensile tests, scanning electron microscopy (SEM) and transmission electron microscopy (TEM). The ultimate tensile strength of the peak-aged Al−Zn−Mg−Cu alloy is improved by about 105 MPa with the addition of 0.10% Zr. An increase of about 133 MPa is observed with the joint addition of 0.07% Sc and 0.07% Zr. For the alloys modified with the minor addition of Sc and Zr (0.14%), the main strengthening mechanisms of minor addition of Sc and Zr are fine-grain strengthening, sub-structure strengthening and the Orowan strengthening mechanism produced by the $Al_3(Sc,Zr)$ and Al_3Zr dispersoids. The volume of Al_3Zr particles is less than that of $Al_3(Sc,Zr)$ particles, but the distribution of $Al_3(Sc,Zr)$ particles is more dispersed throughout the matrix leading to pinning the dislocations motion and restraining the recrystallization more effectively.

Key words: Al−Zn−Mg−Cu alloys; $Al_3(Sc,Zr)$; Al_3Zr; dislocation motion; recrystallization; strengthening mechanism; mechanical properties; microstructure evolution

1 Introduction

Al−Zn−Mg−Cu alloys have been widely used in the aircraft and transportation industries due to their high strength and toughness [1,2]. The GP zones and fine dispersed η'-precipitates ($MgZn_2$) are the primary strengthening phases of peak aged (PA) Al−Zn−Mg−Cu alloys [3]. Moreover, Cu element as the primary alloying element can greatly improve the tensile strength of alloys and make the precipitated phase distribute more dispersively [4]. Trace additions of Sc and Zr have great potential to develop Al alloys with excellent strength and plasticity [5−9]. Minor additions of Sc and Zr to the Al−Zn−Mg−Cu alloys can simultaneously help the alloys achieve higher strength and ductility, due to the formation of dispersive $L1_2$-structured $Al_3(Sc,Zr)$ particles during the homogenization process. The $Al_3(Sc,Zr)$ particles can effectively hinder the recrystallization, inhibit the grain growth and improve the mechanical properties of the alloys [10−12]. Sc is a transition element that has been used to replace Ti/TiB [13] as an effective grain refining agent for many years. Primary Al_3Sc particles can be used for excellent heterogeneous nucleation, which can thereby effectively refine the grain size in the solidification process of aluminum alloy [14,15]. In the Al−Sc binary system, the recrystallization can be effectively retained with the addition of 0.15%−0.20% Sc [16−18].

In Al−0.06Sc−0.06Zr alloy, KNIPLING et al [19] observed that the precipitation of Zr-enriched shell onto the core containing Al and Sc

Foundation item: Project (2016B090931004) supported by the Scientific and Research Plan of Guangdong Province, China; Project (51601229) supported by the National Natural Science Foundation of China
Corresponding author: Guo-fu XU; Tel/Fax: +86-731-88877217; E-mail: csuxgf660302@csu.edu.cn
DOI: 10.1016/S1003-6326(20)65308-0

led to a strength increase, and the peak microhardness was 618 MPa at 400 °C. MUKHOPADHYAY et al [20] indicated that after the joint addition of 0.23% Sc and 0.14% Zr, the total elongation of the Al−Zn−Mg−Cu alloys can reach 916%, showing an excellent superplasticity. DENG et al [21] focused on the effects of different ratios of Sc and Zr on the Al−Zn−Mg alloys and found that the yield strength of the T6-treated Al−Zn−Mg−Cu alloy was improved by 66 MPa with the addition of 0.25% Sc and 0.10% Zr. VLACH et al [22] found that fine coherent Al_3(Sc,Zr) particles precipitated during hot extrusion at 350 °C, and Zr solute began to migrate above 240 °C, forming Al_3(Sc,Zr) particles with $L1_2$ structure. In addition, the addition of Sc and Zr also affected the vacancy concentration in the alloy [23]. TANG et al [24] reported after 16 passes of equal channel angular pressing and cold rolling, Al−Mg−Sc−Zr alloy obtained a unique bimodal grain structure composed of ultrafine grains (less than 150 nm) with high dislocation density and fine grains (200−500 nm), with high yield strength of 550 MPa and high tensile strength of 560 MPa.

Though Sc is effective in improving the strength of the Al−Zn−Mg−Cu alloys, it is not economically practical to increase the content of scandium in industrial production, because scandium is costly. Fortunately, the addition of small amounts of Zr can significantly reduce the Sc content required for strengthening Al−Zn−Mg−Cu alloys [10,25,26]. This drived researchers to explore the minimum addition of the expensive element (Sc), while maintaining the desirable strengthening effects. There has far been very little research into the effects of adding Sc and Zr below 0.2%. Thus, the main objective of this study was to explore the effects of Sc and Zr joint addition (0.14%) and Zr addition (0.1%) on the mechanical properties, recrystallization, and precipitation behavior of Al−Zn−Mg−Cu alloys.

2 Experimental

Table 1 lists the chemical compositions of alloys. The as-cast alloys were homogenization treated at 470 °C for 24 h. The homogenized ingots were preheated at 400 °C for 6 h before extrusion in a 1250 t horizontal extruder. The temperature of the extrusion cylinder was 400−420 °C, and the speed of the ingot extrusion master cylinder was 0.5−1.2 mm/s with an extrusion ratio of 22:1. After hot extrusion treatment (HET), they were subjected to solution treatment (ST) at 470 °C for 1 h, followed by quenching and aging at 120 °C for 24 h [27]. Hardness measurements were carried out on a THV−5 digital display Vickers hardness tester, under an applied load of 9.807 N for 15 s. Tensile tests were performed on an MTS 810 testing machine (INSTRON, USA) according to ASTM B557 at a strain rate of 0.01 s^{-1}. EBSD analysis was performed using a Sirion 200 field emission gun scanning electron microscope (SEM) equipped with an EBSD system. Additionally, more detailed observations of the precipitates were made using a TECNAIG2 20 transmission electron microscope (TEM). In this work, the data about the particle size and precipitation free zone width were measured with imagej2x software, and then their average values were taken. In order to reduce the natural aging of the alloys, the thin foils for TEM observation were prepared immediately after heat treatment. The preparation of the foil took about 30 min. Thin foils for EBSD and TEM observations were prepared by twin-jet electron-polishing at 20 V in a solution of 30% nitric acid and 70% methanol cooled to −20 °C. A low angle boundary (LAB) was defined as misorientation between 2° and 15°, and a high angle boundary (HAB) was defined as misorientation greater than 15°. The grain size was calculated by the OIM software.

Table 1 Chemical composition of alloys (wt. %)

Alloy	Zn	Mg	Cu	Sc	Cr	Zr	Ti	Fe	Al
A	7.51	1.57	1.61	−	0.06	−	0.05	0.12	Bal.
B	7.92	1.47	1.49	−	0.06	0.10	0.06	0.10	Bal.
C	7.36	1.47	1.51	0.07	0.05	0.07	0.05	0.10	Bal.

3 Results and discussion

3.1 Microstructure evolution in Al−Zn−Mg−Cu−(Sc)−Zr alloys

Figure 1 displays the bright field TEM images that illustrate the precipitates of the three PA alloys under different conditions.

It can be seen from Fig. 1(a) that there are a large number of coarse rod-like precipitates within the grains and at the grain boundaries in Alloy A after HET. Figure 1(b) shows that coarse second

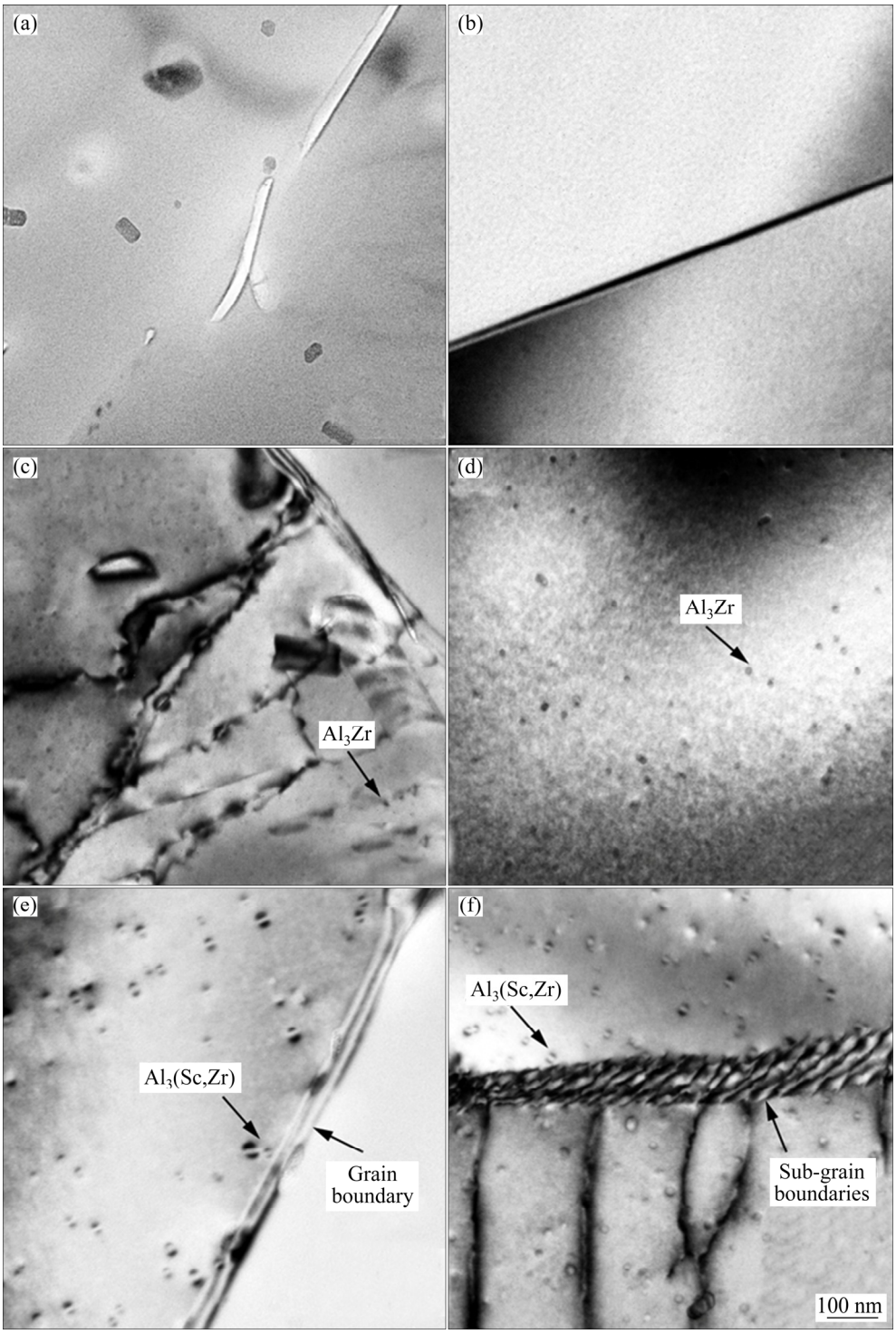

Fig. 1 Bright field TEM images of precipitates in alloys with different treatments: (a) Heat extrusion treated (HET) Alloy A; (b) Solution treated (ST) Alloy A; (c) HET Alloy B; (d) ST Alloy B; (e) HET Alloy C; (f) ST Alloy C

phases and precipitates disappear and dissolve in the matrix after ST. Figure 1(c) demonstrates that, in contrast with Alloy A, a large number of sub-structures remain and coarse rod-like precipitates are observed in Alloy B after HET. There are also spherical and dispersive second phase particles in Alloy B after ST (Fig. 1(d)). Figure 1(e) shows that the particles in Alloy A present Ashby−Brown contrast in bright-field image, indicating that these particles are coherent with the matrix. Moreover, these particles pin the grain boundaries during the heat treatment process,

leading to effective grain refinement. Figure 1(f) shows that these dispersive particles resist the dislocation motion, and hence the sub-grains remain after ST in Alloy C.

Figure 2 presents the dark field TEM images that show the distribution and size of the particles in Alloy B and Alloy C. It can be confirmed that these spherical particles are Al_3Zr particles in Alloy B. Moreover, the Al_3Zr particles pin the immigration of dislocations during HET. It is notable that the distribution of Al_3Zr particles is not homogenous, especially near the grain boundaries, as seen in Figs. 2(b, c). Figure 2(d) shows that the second phase particles disperse homogenously in the matrix during HET in Alloy C. These particles are $Al_3(Sc,Zr)$ particles coherent with the matrix. Figure 2(f) shows that the $Al_3(Sc,Zr)$ particles still exhibit homogenous distribution after solution-aging treatment. These $Al_3(Sc,Zr)$ particles can effectively pin the grain boundaries and suppress the recrystallization during the heat treatment. Furthermore, the volume of Al_3Zr particles is about 63% that of $Al_3(Sc,Zr)$ particles (Figs. 6(g, h)). However, compared with the $Al_3(Sc,Zr)$ particles, the distribution of the Al_3Zr particles is not homogenous, especially near the grain boundaries.

The grain structures of the three (peak-aged) PA alloys are observed using TEM and the results are shown in Fig. 3. Compared with the microstructures of Alloy A in Fig. 3(a), the grain

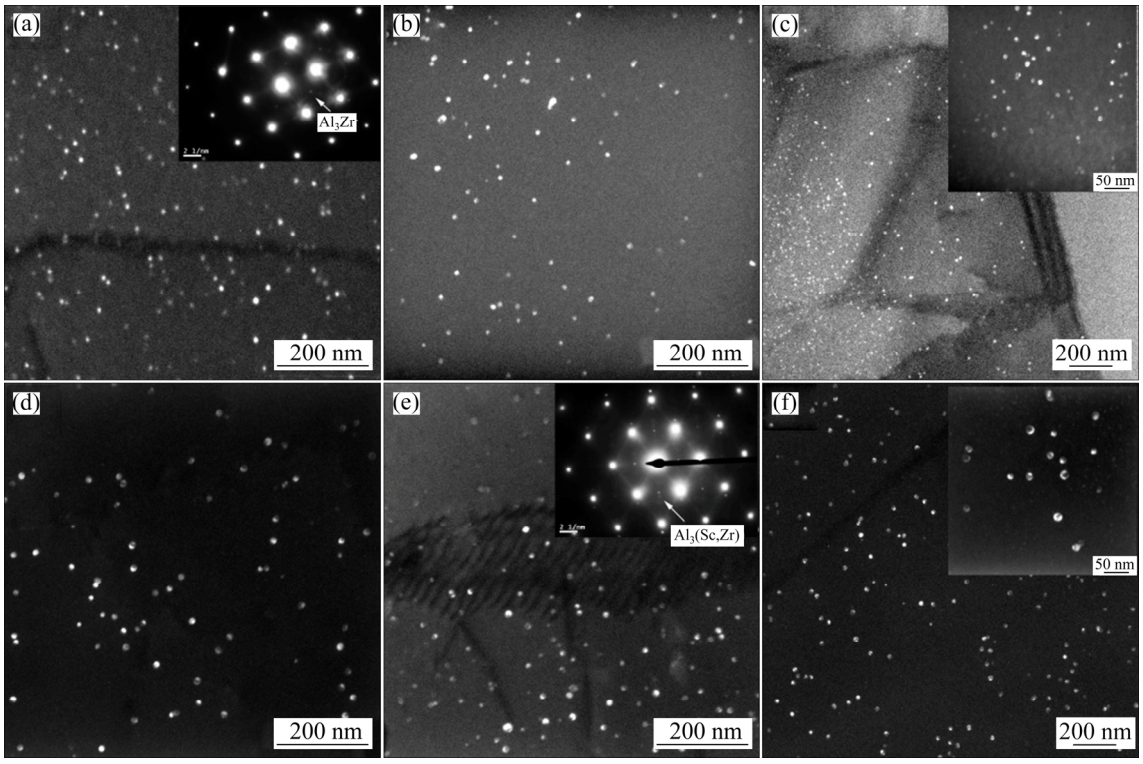

Fig. 2 Dark field TEM images of Alloy B and Alloy C with different treatments: (a) HET Alloy B; (b) ST Alloy B; (c) Peak aged (PA) Alloy B; (d) HET Alloy C; (e) ST Alloy C; (f) PA Alloy C

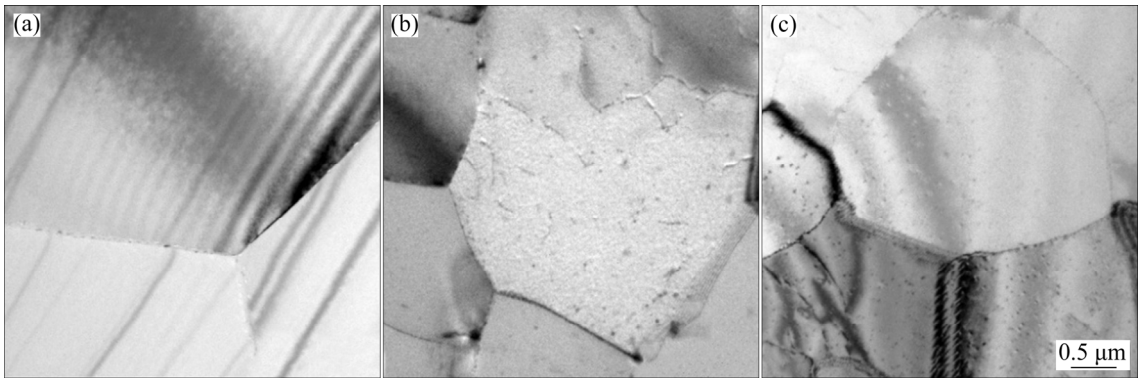

Fig. 3 Bright field TEM images of three alloys under peak aged condition: (a) Alloy A; (b) Alloy B; (c) Alloy C

sizes are much smaller (Figs. 3(b, c)) in Alloys B and C. Moreover, the sub-grains and dislocation can also be seen in the solution-aging treated Alloy C. Hence, the substructures effectively remain and the grains are significantly refined due to the joint addition of Sc and Zr.

The EBSD images of the three HET and ST Al−Zn−Mg−Cu alloys are shown in Fig. 4. It can be seen that most of the grain boundaries of Alloy A, without Sc and Zr addition, are characterized by high angle grain boundaries, indicating that complete recrystallization has occurred in Alloy A after heat extrusion treatment (Fig. 4(a) and Fig. 5). HET Alloy B and Alloy C exhibit highly elongated grain structures along the extrusion direction, with a large number of fiber-like structures consisting of sub-grains characterized by low angle grain boundaries as shown in Figs. 4 (b, c). Figure 4(d) shows that coarse grains are the dominant grain structures in Alloy A, with mean grain size of (27±8) μm after ST. Figure 4(e) illustrates that the elongated grain structures disappear and apparent recrystallization occurs in Alloy B after ST. Compared with the ST Alloy A, the mean grain size in the ST Alloy B decreases from (27±8) to (14±7) μm when modified with 0.1% Zr. Figure 4(f) presents the grain structures of Alloy C after ST. Different from the ST Alloy A and Alloy B, the mean grain size further decreases to (6±5) μm in Alloy C modified with 0.07% Sc and 0.07% Zr after ST. Additionally, the grain structures of Alloy C present a mixture of highly elongated grains and fiber-like structures. Ultrafine equiaxed grains along the ED are observed in Alloy A after ST, indicating the occurrence of partial recrystallization. The above results demonstrate that joint addition of 0.07% Sc and 0.07% Zr leads to the formation of dispersive $Al_3(Sc,Zr)$ particles which effectively

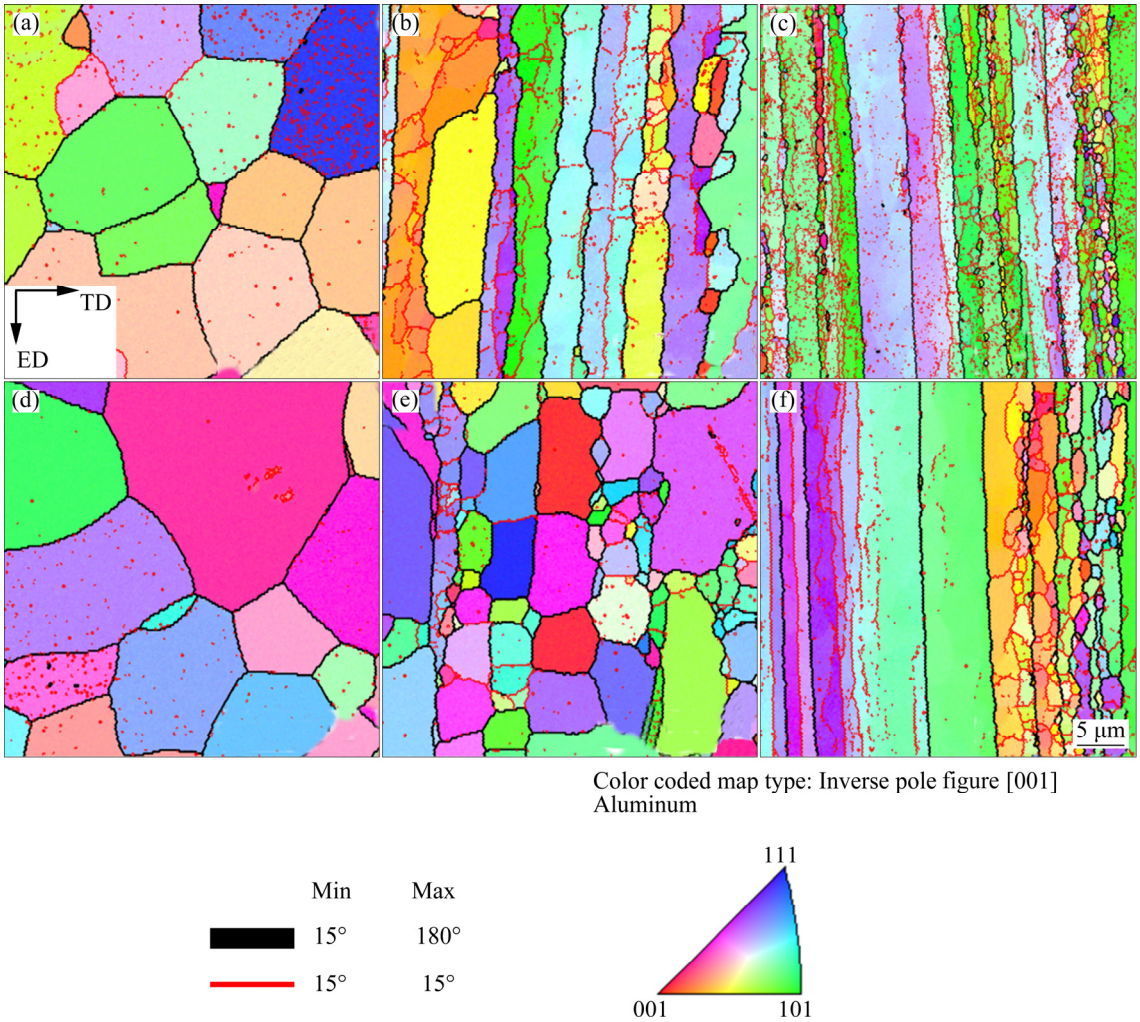

Fig. 4 EBSD maps of three alloys: (a) HET Alloy A; (b) HET Alloy B; (c) HET Alloy C; (d) ST Alloy A; (e) ST Alloy B; (f) ST Alloy C

inhibit the recrystallization. Meanwhile, the addition of 0.10% Zr is less effective in terms of inhibiting recrystallization compared with the joint addition of Sc and Zr (Fig. 5), and many elongated structures can be seen in the matrix of Alloy C.

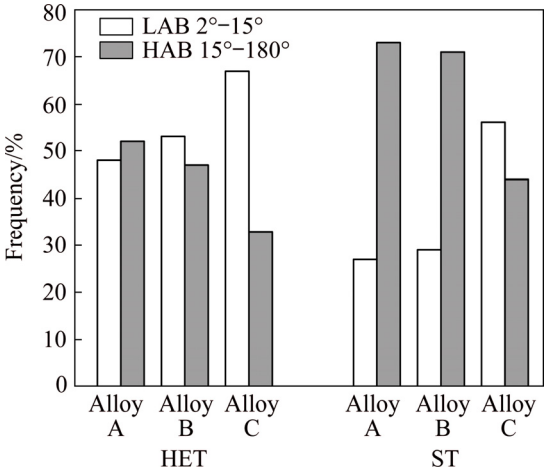

Fig. 5 Misorientation angle distributions in three alloys with different treatments

3.2 Aging precipitates in Al−Zn−Mg−Cu(−Sc−Zr) alloys

The TEM images of aging precipitates in the three alloys under different conditions are shown in Fig. 6. Many η-$MgZn_2$ precipitates homogenously disperse within the grains in PA alloys. It is notable that the coarse rod-like aging precipitates segregate at the grain boundaries and the width of the precipitation free zones is 33 nm (Fig. 6(a)). The precipitates along the grain boundaries are continuous in Alloys B and C, but there are almost no differences in the distribution and coarsening degree of phases within the grains (Figs. 6(b, c)). Moreover, the precipitates of Alloy C at the grain boundaries are finer than those of Alloy B. Therefore, it can be inferred that the additions of Sc and Zr have no effects on the size and density of the aging precipitates within the grains. Nevertheless, aging precipitates are markedly refined and the width of the free precipitation zones is reduced along the grain boundaries.

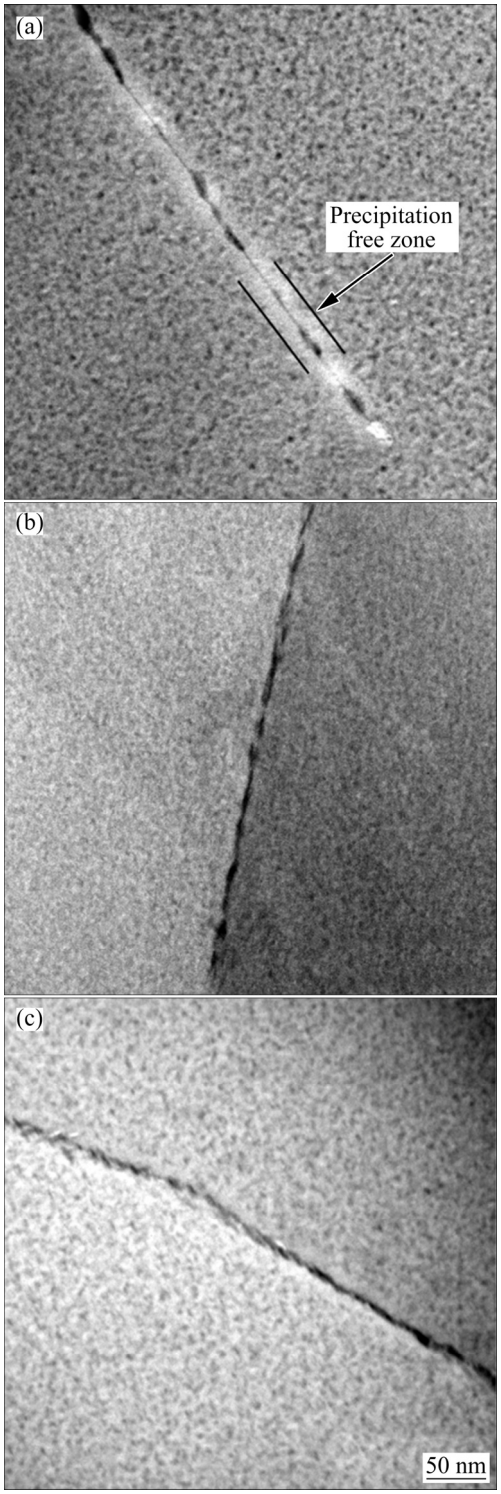

Fig. 6 Bright field TEM images of three alloys aged at 120 °C: (a) Alloy A; (b) Alloy B; (c) Alloy C

Figure 7 shows the variation of hardness with time during aging at 120 °C for the three alloys. It is obvious that the hardness values of the three alloys markedly increase during under-aging and decrease during over-aging. The hardness of Alloy C is higher than that of Alloys A and B. The initial hardness values are HV (64.9±1.3), (74.0±0.2) and (77.5±0.3) for Alloys A, B and C in ST state, respectively, and then increase to HV (168.7±2.5), (172.0±2.2) and (177.1±0.8) after artificial aging at 120 °C for 24 h. Moreover, the improvement of hardness by the addition of Sc and Zr affects the whole aging process, and the alloys are all in PA

state after 24 h aging at 120 °C. Combined with the TEM images of the three alloys (Fig. 5), it can be inferred that minor additions of Sc and Zr do not retard and suppress the precipitation behavior of the aging precipitates.

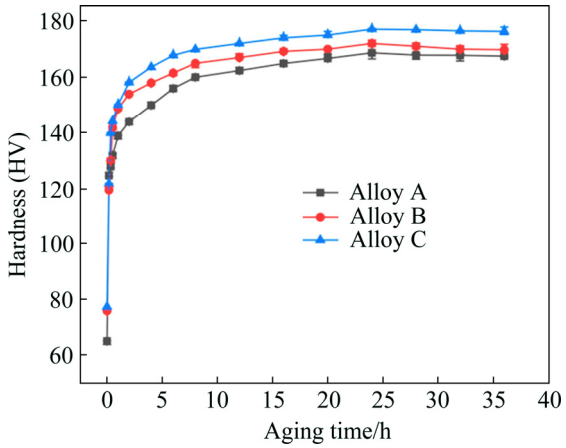

Fig. 7 Aging curves of three alloys at 120 °C

3.3 Tensile properties and strengthening mechanisms in Al−Zn−Mg−Cu(−Sc−Zr) alloys

Figure 8 shows the tensile properties of alloys under different conditions. The yield strengths (YS) of ST Alloys A, B and C are about 145, 175 and 198 MPa, and the ultimate tensile strengths (UTS) are about 286, 348 and 365 MPa, respectively. Moreover, after T6-treatment, the YS of Alloys A, B and C increases by about 299, 369 and 401 MPa, and the UTS increases by about 234, 278 and 288 MPa, respectively. The UTS of the T6-treated base alloy improves by about 105 MPa with the addition of 0.1% Zr and by about 133 MPa with the addition of 0.07% Sc and 0.07% Zr. It can be inferred that the joint minor addition of Sc and Zr can more effectively enhance the mechanical properties than the minor addition of Zr only. Furthermore, the strengthening from Sc and Zr micro-alloying is independent from that by age hardening in the Al−Zn−Mg−Cu alloys.

As described in Table 2, the contents of Sc and Zr added to the Al−Zn−Mg−Cu alloys are above 0.2% in previous investigations. Although the content of Sc and Zr is decreased to 0.14% in this work, Alloy A still exhibits high strength and promising ductility. Furthermore, the strength increase from the Orowan strengthening of secondary $Al_3(Sc,Zr)$ particles is much higher than that from the fine-grain strengthening of primary $Al_3(Sc,Zr)$ particles [22]. Primary $Al_3(Sc,Zr)$ particles can also cause stress concentration and promote fracture, leading to a drop in ductility. However, after adding a trace amount of Sc and Zr, secondary $Al_3(Sc,Zr)$ particles form after homogenization and subsequent heat treatment [28]. These particles effectively anchor the grain boundaries and impede the appearance and growth of sub-grains [32,33]. Primary $Al_3(Sc,Zr)$ particles rarely form in alloys with a low content of Sc and Zr. Therefore, Alloy A, modified with 0.14% Sc and Zr, is distinguished by possessing higher mechanical properties than the other two alloys.

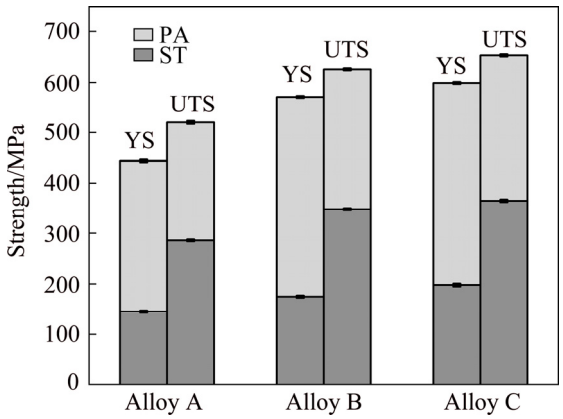

Fig. 8 Tensile properties of three alloys under different conditions

Most $Al_3(Sc,Zr)$ particles precipitate from supersaturated solution matrices [34], and secondary $Al_3(Sc,Zr)$ particles are dispersive and coherent with the matrix. According to the Orowan mechanism, dislocations consume energy to span secondary $Al_3(Sc,Zr)$ particles, with more energy being consumed for smaller and more dispersive particles. The binary Al−Zr equilibrium phase diagram shows that the peritectic reaction dominates the aluminum-rich end and the solid solubility is about 0.28% when the liquid phase is in equilibrium with the Al_3Zr inter-metallic phase and Zr [35]. Under non-equilibrium conditions, the solid solubility of solidified Zr may reach 2.0%−2.5%. In this work, the presence of Ashby−Brown contrast in bright field image is rarely detected. According to Zener formula [36], in the case of second phase particles under the same volume fraction, smaller particles are more effective in pinning dislocations and impeding grain boundary migrations. However, in this work, compared with the $Al_3(Sc,Zr)$ particles, the

Table 2 Tensile properties of Al−Zn−Mg−Cu alloys with Sc and Zr additions at different states

Alloy composition/wt.%	State	Tensile properties			Ref.
		YS/MPa	UTS/MPa	Elongation/%	
Al−7.36Zn−1.47Mg−1.51Cu−0.07Sc−0.07Zr	ST	198	365	15.0	This study
Al−5.36Zn−1.90Mg−0.25Cu−0.10Sc−0.10Zr	ST	252	378	15.0	[19]
Al−5.4Zn−1.98Mg−0.33Cu−0.25Sc−0.10Zr	ST	275	397	23.3	[28]
Al−7.36Zn−1.47Mg−1.51Cu−0.07Sc−0.07Zr	PA	599	653	11.0	This study
Al−8.25Zn−2.10Mg−2.21Cu−0.10Sc−0.18Zr	PA	573	630	12.6	[29]
Al−7.17Zn−2.20Mg−1.58Cu−0.18Sc−0.18Zr	PA	523	613	8.6	[30]
Al−5.41Zn−1.98Mg−0.33Cu−0.25Sc−0.10Zr	PA	535	556	12.1	[26]
Al−6.20Zn−2.30Mg−1.0Cu−0.36(Sc + Zr)	PA	602	640	13.8	[31]
Al−8.07Zn−2.04Mg−2.32Cu−0.29Sc−0.13Zr	PA	600	645	9.0	[15]
Al−8.10Zn−2.06Mg−2.33Cu−0.49Sc−0.11Zr	PA	574	633	10.5	[15]

distribution of the Al_3Zr particles is not homogenous, especially near the grain boundaries. Therefore, the $Al_3(Sc,Zr)$ particles can more effectively inhibit the recrystallization, thereby improving the mechanical properties, which is consistent with the tensile test results. Additionally, according to the standard Hall−Petch equation, yield strength is related to mean grain size. In this equation, as the mean grain size decreases, the yield strength increases. The mean grain sizes are about 27, 14 and 6 μm for Alloys A, B and C, respectively. The YS of ST Alloy A increases by about 30 and 54 MPa after adding 0.1% Zr and 0.07% Sc plus 0.07% Zr, respectively. As determined by the EBSD and mechanical property results, it can be concluded that the joint addition of Sc and Zr, through dispersive distribution and coherent structure of $Al_3(Sc,Zr)$ particles, can more effectively refine the grain structures in the Al−Zn−Mg−Cu alloys, leading to higher mechanical properties than those of alloys with the addition of Zr alone. Moreover, the joint addition of Sc and Zr can efficiently retain the sub-structures (Fig. 3(c) and Fig. 4(f)), which can markedly improve the mechanical properties of the Al−Zn−Mg−Cu alloys. Therefore, the sub-structure strengthening mechanism is one of the strengthening mechanisms of Sc and Zr micro-alloying. This result indicates that the addition of Sc and Zr can improve the age strengthening effect, due to the refinement of the precipitates at the grain boundaries, and reduce the width of PFZ. Moreover, the YS increase from aging precipitation is much higher than that from minor Sc and Zr addition.

Altogether, it can be inferred that the joint minor addition of Sc and Zr can effectively hinder the recrystallization and increase the mechanical properties of the alloys. The fine dispersive secondary $Al_3(Sc,Zr)$ particles which are coherent with the matrix during heat treatment process, act to refine the grain size [11,29,37]. Moreover, the dispersive distribution of particles promotes the stabilization of sub-structures during deformation and heat treatment process, which then effectively improves the mechanical properties. Because of the different sizes of particles, the strengthening effect caused by the second phase particles is attributed to two mechanisms: the shearing and the Orowan bypass mechanisms. Moreover, with the increase of particle diameter, the strengthening mechanism of yield strength is gradually changed from the shearing mechanism to the Orowan mechanism when the particle diameter is 4−6 nm [30]. This indicates that the Orowan mechanism is the main mechanism for the strengthening from Al_3Zr particles with an average size of ~18 nm and $Al_3(Sc,Zr)$ particles with an average size of ~21 nm. The yield strength of the PA alloy increases by about 30 and 53 MPa, respectively, with the addition of Zr and joint addition of Sc and Zr, owing to the fine-grain strengthening, the sub-structure strengthening and the Orowan strengthening mechanisms caused by $Al_3(Sc,Zr)$ and Al_3Zr particles.

4 Conclusions

(1) The ultimate tensile strength improves by

about 105 MPa after adding 0.10% Zr and by about 133 MPa after adding 0.07% Zr and 0.07% Sc. The strengthening mechanisms of adding Sc and Zr are the fine-grain strengthening, the sub-structure strengthening and the Orowan strengthening mechanisms.

(2) The minor addition of Sc and Zr leading to the formation of $Al_3(Sc,Zr)$ or Al_3Zr particles produces refinement in aging precipitates at the grain boundaries of the Al−Zn−Mg−Cu alloys, but it does not promote or suppress the precipitation behavior of the aging precipitates.

(3) The volume of $Al_3(Sc,Zr)$ particles is larger than that of Al_3Zr particles. However, the distribution of the $Al_3(Sc,Zr)$ particles is more homogenous. The joint addition of 0.07% Zr and 0.07% Sc can more effectively resist the recrystallization and improve the mechanical properties of the Al−Zn−Mg−Cu alloys than the addition of 0.10% Zr only.

References

[1] PENG X Y, GUO Q, LIANG X P, DENG Y, GU Y, XU G F, YIN Z M. Mechanical properties, corrosion behavior and microstructures of a non isothermal ageing treated Al−Zn−Mg−Cu alloy [J]. Materials Science and Engineering A, 2017, 688: 146−154.

[2] ZHANG Y D, JIN S B, TRIMBY P W, LIAO X Z, MURASHKIN X M, VALIEV R Z, LIU J, CAIRNEY J M, RINGER S P, SHA G. Dynamic precipitation, segregation and strengthening of an Al−Zn−Mg−Cu alloy (AA7075) processed by high-pressure torsion [J]. Acta Materialia, 2019, 162: 19−32.

[3] PENG X Y, LI Y, LIANG X P, GUO Q, XU G F. Precipitate behavior and mechanical properties of enhanced solution treated Al−Zn−Mg−Cu alloy during non-isothermal ageing [J]. Journal of Alloys and Compounds, 2018, 735: 964−974.

[4] DONG P X, CHEN S Y, CHEN K H. Effects of Cu content on microstructure and properties of super-high-strength Al−9.3Zn−2.4Mg−*x*Cu−Zr alloy [J]. Journal of Alloys and Compounds, 2019, 788: 329−337.

[5] DUAN Y L, XU G F, PENG X Y, DENG Y, LI Z, YIN Z M. Effect of Sc and Zr additions on grain stability and superplasticity of the simple thermal-mechanical processed Al−Zn−Mg alloy sheet [J]. Materials Science and Engineering A, 2015, 648: 80−91.

[6] CAO X W, XU G F, DUAN Y L, YIN Z M, LU L Y, WANG Y J. Achieving high superplasticity of a new Al−Mg−Sc−Zr alloy sheet prepared by a simple thermal-mechanical process [J]. Materials Science and Engineering A, 2015, 647: 333−343.

[7] DUAN Y L, XU G F, XIAO D, ZHOU L Q, DENG Y, YIN Z M. Excellent superplasticity and deformation mechanism of Al−Mg−Sc−Zr alloy processed via simple free forging [J]. Materials Science and Engineering A, 2015, 624: 124−131.

[8] XU G F, CAO X W, ZHANG T, DUAN Y L, PENG X Y, DENG Y, YIN Z M. Achieving high strain rate superplasticity of an Al−Mg−Sc−Zr alloy by a new asymmetrical rolling technology [J]. Materials Science and Engineering A, 2016, 672: 98−107.

[9] PENG Y Y, LI S, DENG Y, ZHOU H, XU G F, YIN Z M. Synergetic effects of Sc and Zr microalloying and heat treatment on mechanical properties and exfoliation corrosion behavior of Al−Mg−Mn alloys [J]. Materials Science and Engineering A, 2016, 666: 61−71.

[10] ZOU L, PAN Q L, HE Y B, WANG C Z, LIANG W J. Effect of minor Sc and Zr addition on microstructures and mechanical properties of Al−Zn−Mg−Cu alloys [J]. Transactions of Nonferrous Metals Society of China, 2007, 17(2): 340−345.

[11] YIN Z M, YANG L, PAN Q L, JIANG F. Effect of minor Sc and Zr on microstructures and mechanical properties of Al−Zn−Mg based alloys [J]. Transactions of Nonferrous Metals Society of China, 2011, 11(6): 822−825.

[12] TZENG Y C, WU C T, LEE S L. The effect of trace Sc on the quench sensitivity of Al−7Si−0.6 Mg alloys [J]. Materials Letters, 2015, 161: 340−342.

[13] FENG J, YE B, ZUO L J, QI R J, WANG Q D, JIANG H Y, HUANG R. Effects of Zr, Ti and Sc additions on the microstructure and mechanical properties of Al−0.4Cu−0.14Si−0.05Mg−0.2Fe alloys [J]. Journal Of Materials Science and Technology, 2018, 34(12): 2316−2324.

[14] HUANG X, PAN Q L, LI B, LIU Z M, HUANG Z Q, YIN Z M. Effect of minor Sc on microstructure and mechanical properties of Al−Zn−Mg−Zr alloy metal-inert gas welds [J]. Journal of Alloys and Compounds, 2015, 629: 197−207.

[15] LI W B, PAN Q L, ZOU L, LIANG W J, HE Y B, LIU J S. Effects of minor Sc on the microstructure and mechanical properties of Al−Zn−Mg−Cu−Zr based alloys [J]. Rare Metals, 2009, 28(1): 102−106.

[16] MARQUIS E A, SEDMAN D N, DUNAND D C. Precipitation strengthening at ambient and elevated temperatures of heat-treatable Al(Sc) alloys [J]. Acta Materialia, 2002, 51(1): 285−287.

[17] NOVOTNY G M, ARDELL A J. Precipitation of Al_3Sc in binary Al−Sc alloys[J]. Materials Science and Engineering A, 2001, 318: 144−154.

[18] MURRAY J L. The Al−Sc (aluminum−scandium) system [J]. Journal of Phase Equilibria, 1998, 19(4): 380−384.

[19] KNIPLING K E, SEIDMAN D N, DUNAND D C. Ambient- and high-temperature mechanical properties of isochronally aged Al−0.06Sc, Al−0.06Zr and Al−0.06Sc−0.06Zr (at.%) alloys [J]. Acta Materialia, 2011, 59(3): 943−954.

[20] MUKHOPADHYAY A K, KUMAR A, RAVEENDRA S, SAMAJDAR I. Development of grain structure during superplastic deformation of an Al−Zn−Mg−Cu−Zr alloy containing Sc [J]. Scripta Materialia, 2011, 64(5): 386−389.

[21] DENG Y, YIN Z M, ZHAO K, DUAN J Q, HE Z B. Effects of Sc and Zr microalloying additions on the microstructure and mechanical properties of new Al−Zn−Mg alloys [J]. Journal of Alloys and Compounds, 2012, 530: 71−80.

[22] VLACH M, CIZEK J, SMOLA B, STULIKOVA I, HRUSKA P, KODETOVA V, DANIS S, TANPRAYOON D,

NEUBERT V. Influence of dislocations on precipitation processes in hot-extruded Al−Mn−Sc−Zr alloy [J]. International Journal of Materials Research, 2018, 109(7): 583−592.

[23] Vlach M, KODETOVA V, SMOLA B, CIZEK J, KEKULE T, CIESLAR M. Characterization of phase development in commercial Al−Zn−Mg(−Mn, Fe) alloy with and without Sc, Zr-addition [J]. Kovove Mater, 2018, 56: 367−377.

[24] TANG L, XU G F, DENG Y, GAN H, MA A B, YIN Z M. Mechanical properties and microstructure of an Al−Zn−Mg−Sc−Zr alloy processed by warm equal channel angular pressing and subsequent aging [J]. JOM, 2018, 70(11): 2684−2691.

[25] LIU J, YAO P, ZHAO N Q, SHI C S, LI H J, LI X, XI D S, YANG S. Effect of minor Sc and Zr on recrystallization behavior and mechanical properties of novel Al−Zn−Mg−Cu alloys [J]. Journal of Alloys and Compounds, 2016, 657: 717−725.

[26] SENKOV O N, SENKOVA S V, SHAGIEV M R. Effect of Sc on aging kinetics in a direct chill cast Al−Zn−Mg−Cu alloy [J]. Metallurgical and Materials Transactions A, 2008, 39(5): 1034−1053.

[27] QIN C, GOU G Q, CHE X L, CHEN H, CHEN J, LI P, GAO W. Effect of composition on tensile properties and fracture toughness of Al−Zn−Mg alloy (A7N01S-T5) used in high speed trains [J]. Materials and Design, 2016, 91: 278−285.

[28] TANG L, PENG X Y, HUANG J W, MA A B, DENG Y, XU G F. Microstructure and mechanical properties of severely deformed Al−Mg−Sc−Zr alloy and their evolution during annealing [J]. Materials Science and Engineering A, 2019, 754: 295−308.

[29] FULLER C B, SEIDMAN D N, DUNAND D C. Mechanical properties of Al(Sc,Zr) alloys at ambient and elevated temperatures [J]. Acta Materialia, 2003, 51(16): 4803−4814.

[30] HE Y D, ZHANG X M, YOU J H. Effects of minor contents of Sc and Zr on microstructure and mechanical properties of Al−Zn−Mg−Cu alloy [J]. Rare Metal Materials and Engineering, 2007, 36(4): 665−670. (in Chinese)

[31] SENKOV O N, SHAGIEV M R, SENKOVA S V, MIRACLE D B. Precipitation of Al(Sc,Zr) particles in an Al−Zn−Mg−Cu−Sc−Zr alloy during conventional solution heat treatment and its effect on tensile properties [J]. Acta Materialia, 2008, 56(15): 3723−3738.

[32] DUAN Y L, TANG L, DENG Y, CAO X W, XU G F, YIN Z M. Superplastic behavior and microstructure evolution of a new Al−Mg−Sc−Zr alloy subjected to a simple thermomechanical processing [J]. Materials Science and Engineering A, 2016, 669: 205−217.

[33] YIN Z M, PAN Q L, ZHANG Y H, JIANG F. Effect of minor Sc and Zr on the microstructure and mechanical properties of Al−Mg based alloys [J]. Materials Science and Engineering A, 2000, 280: 151−155.

[34] DORWARD R C, BEERNTSEN D. Grain structure and quench-rate effects on strength and toughness of AA7050 Al−Zn−Mg−Cu−Zr alloy plate [J]. Metallurgical and Materials Transactions A, 1995, 26(9): 2481−2484.

[35] TALEGHANI M A J, NAVAS E M R, SALEHI M, TORRALBA J M. Hot deformation behaviour and flow stress prediction of 7075 aluminium alloy powder compacts during compression at elevated temperatures [J]. Materials Science and Engineering A, 2012, 534: 624−631.

[36] DUAN Y L, XU G F, TANG L, LIU Y, XU J W, DENG Y, YIN Z M. Excellent high strain rate superplasticity of Al−Mg−Sc−Zr alloy sheet produced by an improved asymmetrical rolling process [J]. Journal of Alloys and Compounds, 2017, 715: 311−321.

[37] DUAN Y L, QIAN J, XIAO D, CUI X M, XU G F. Effect of Sc and Er additions on superplastic ductilities in Al−Mg−Mn−Zr alloy [J]. Journal of Central South University, 2016, 23(6): 1283−1292.

添加微量 Sc 和 Zr 对 Al−Zn−Mg−Cu 合金力学性能和显微组织演变的影响

肖权峰[1]，黄继武[1,2]，蒋莺歌[1]，江福清[1]，吴昀峰[1]，徐国富[1,2]

1. 中南大学 材料科学与工程学院，长沙 410083；
2. 中南大学 有色金属材料科学与工程教育部重点实验室，长沙 410083

摘　要：采用拉伸试验、扫描电镜和透射电镜，研究添加微量 Sc 和 Zr 对 Al−Zn−Mg−Cu 合金力学性能和显微组织演变的影响。添加 0.10% Zr 使合金的抗拉强度提高约 105 MPa, 而复合添加 0.07% Sc 和 0.07% Zr 使合金抗拉强度提高约 133 MPa。在峰时效状态的合金中，添加微量 Sc 和 Zr 的主要强化机制是 $Al_3(Sc,Zr)$和 Al_3Zr 粒子引起的细晶强化、亚晶强化和奥罗万强化。$Al_3(Sc,Zr)$颗粒的尺寸大于 Al_3Zr 颗粒的尺寸，但 $Al_3(Sc,Zr)$粒子分布更加弥散，因此，$Al_3(Sc,Zr)$粒子能更加有效钉扎位错运动和抑制再结晶。

关键词：Al−Zn−Mg−Cu 合金；$Al_3(Sc,Zr)$；Al_3Zr；位错运动；再结晶；强化机制；力学性能；显微组织演变

(Edited by Bing YANG)